Host and viral determinants for efficient SARS-CoV-2 infection of the human lung

Hin Chu
  The University of Hong Kong

Bingjie Hu
  The University of Hong Kong

Xiner Huang
  The University of Hong Kong

Yue Chai
  The University of Hong Kong

Yixin Wang
  The University of Hong Kong

Huiping Shuai
  The University of Hong Kong

Dong Yang
  The University of Hong Kong

Yuxin Hou
  The University of Hong Kong

Xi Zhang
  The University of Hong Kong

Terrence Tsz-Tai Yuen
  The University of Hong Kong

Jian-Piao Cai
  The University of Hong Kong

Anna Jinxia Zhang
  The University of Hong Kong

Jie Zhou
  The University of Hong Kong

Shuofeng Yuan
  The University of Hong Kong

Kelvin Kai-Wang To
  The University of Hong Kong

Ivy Hau-Yee Chan
  The University of Hong Kong

Ko-Yung Sit

The University of Hong Kong

Dominic Chi-Chun Foo
　The University of Hong Kong

Ian Yu-Hong Wong
　The University of Hong Kong

Ada Tsui-Lin Ng
　The University of Hong Kong

Tan To Cheung
　The University of Hong Kong

Simon Ying-Kit Law
　The University of Hong Kong

Wing-Kuk Au
　The University of Hong Kong

Kin-Hang Kok
　The University of Hong Kong

Jasper Fuk-Woo Chan
　The University of Hong Kong

Kwok-Yung Yuen (✉ kyyuen@hku.hk)
　The University of Hong Kong

Abstract

SARS-CoV-2 has affected over 9 million patients with more than 460,000 deaths in about 6 months. Understanding the factors that contribute to efficient SARS-CoV-2 infection of human cells, which are not previously reported, may provide insights on SARS-CoV-2 transmissibility and pathogenesis, and reveal targets of intervention. Here, we reported key host and viral determinants that were essential for efficient SARS-CoV-2 infection in the human lung. First, we identified heparan sulfate as an important attachment factor for SARS-CoV-2 infection. Second, we demonstrated that while cell surface sialic acids significantly restricted SARS-CoV infection, SARS-CoV-2 could largely overcome sialic acid-mediated restriction in both human lung epithelial cells and *ex vivo* human lung tissue explants. Third, we demonstrated that the inserted furin-like cleavage site in SARS-CoV-2 spike was required for efficient virus replication in human lung but not intestine tissues. Overall, these findings contributed to our understanding on efficient SARS-CoV-2 infection of human lungs.

Introduction

Severe acute respiratory syndrome coronavirus 2 (SARS-CoV−2) was first reported from Wuhan, China, in December 2019 [1]. Infection of SARS-CoV−2 results in Coronavirus Disease 2019 (COVID−19), which shares a number of similar clinical manifestations with that of SARS but with a lower mortality rate [2−4]. However, SARS-CoV−2 is highly efficient in person-to-person transmission and has resulted in over 9 million cases with more than 460,000 deaths in 218 countries or regions within approximately 6 months [5,6]. Investigations on the host and viral determinants that contribute to efficient SARS-CoV−2 infection of human cells is a key research question that may facilitate our understanding on the biology of SARS-CoV−2 transmission and pathogenesis.

Successful coronavirus infection requires direct interaction between the coronavirus spike protein and the host cell surface receptor [7,8]. In addition to their protein receptors, coronavirus spikes recognize a broad array of cell surface molecules, which serve to facilitate virus attachment or entry [9−15]. Similar to SARS-CoV and human coronavirus NL63 (HCoV-NL63), the SARS-CoV−2 spike protein recognizes angiotensin-converting enzyme 2 (ACE2) as the cell receptor for entry [16,17]. However, the expression level of ACE2 in the lung and respiratory tract is relatively low in comparison to many other human tissues, suggesting that low levels of ACE2 is biologically relevant in supporting SARS-CoV−2 entry [18]. Alternatively, SARS-CoV−2 may be able to utilize other host determinants along the respiratory tract to facilitate virus infection. In this regard, heparan sulfate and sialic acids are two ubiquitously expressed host factors that are frequently utilized by human and animal coronaviruses for attachment and entry [11−15]. However, their involvement in SARS-CoV−2 infection has not been explored.

In addition to recognition of cell surface molecules by the spike protein for attachment and entry, proteolytic activation of the coronavirus spike protein at the S_1/S_2 and S_2' sites is essential for membrane

fusion and infection of the host cells [8]. Cleavage of spike begins during virus egress along the secretory pathways by proprotein convertases such as furin [19]. Additional spike cleavage occurs during virus entry and is mediated by host proteases including transmembrane protease serine 2 (TMPRSS2) and cathepsin L, which is the representative protease for the plasma membrane entry and endosomal entry pathway, respectively [20–22]. Recent studies identified a four amino acid insertion at the S_1/S_2 junction of SARS-CoV−2 spike that resulted in a "RRAR" sequence, which corresponded to a canonical furin-like cleavage site [23,24]. These residues are absent in the spike protein of SARS-CoV, SARS-CoV-related coronavirus (SARSr-CoV), and the closely related bat coronavirus RaTG13 [25]. The additional furin-like cleavage site is widely postulated to facilitate virus entry and increase cell tropism, leading to efficient virus spread in the human population [23–26]. However, the physiological relevance of this furin-like motif in SARS-CoV−2 spike has not been functionally evaluated during infectious virus infection.

In this study, we investigated the involvement of cell surface heparan sulfate and sialic acids in SARS-CoV−2 infection and evaluated the physiological importance of the inserted furin-like cleavage site in SARS-CoV−2 spike during virus replication. Our results revealed novel information on the host and viral determinants that orchestrated the efficient SARS-CoV−2 infection of the human lungs. These findings contributed to our understanding on the biology of the high SARS-CoV−2 transmissibility and suggested targets of intervention against COVID−19.

Results

Heparan sulfate serves as an essential host determinant during SARS-CoV−2 attachment and replication.

Angiotensin-converting enzyme 2 (ACE2) was identified as the receptor of SARS-CoV−2. Interestingly, ACE2 expression is relatively low in the respiratory tract and SARS-CoV−2 infection could be detected in cells with limited ACE2 expression, suggesting the involvement of additional host determinants in SARS-CoV−2 infection [27,28]. Heparan sulfate proteoglycans were previously identified as the attachment receptors for HCoV-NL63, which served an indispensable role during HCoV-NL63 attachment and infection of target cells [11,29]. Despite both HCoV-NL63 and SARS-CoV−2 utilize ACE2 as the entry receptor, the involvement of heparan sulfate proteoglycans during SARS-CoV−2 entry remain unexplored. To this end, we evaluated the role of heparan sulfate during SARS-CoV−2 infection. We infected Calu3 (lung epithelial) and Caco2 (intestine epithelial) cells with early passage SARS-CoV−2 that were pretreated with heparan sulfate, and harvested samples at 24 hours post infection. Our results showed that the heparan sulfate treatment significantly reduced SARS-CoV−2 replication in both cell lysate and supernatant samples of Calu3 and Caco2 (Fig. 1a,b). Importantly, we further demonstrated that the heparan sulfate treatment reduced SARS-CoV−2 replication in a dose-dependent manner. At 500μg/ml, the treatment substantially reduced the amount of SARS-CoV−2 in the supernatant of Calu3 and Caco2 cells by 96% (p<0.0001) and 99% (p<0.0001), respectively (Fig. 1a,b). Next, to explore the mechanism of exogenous heparan sulfate-mediated SARS-CoV−2 inhibition, we pretreated SARS-CoV−2 with heparan

sulfate for 1 hour before adding the inoculum to Calu3 and Caco2 cells at 4 degree for 2 hours (Fig. 1c). Our data demonstrated that exogenous heparan sulfate pretreatment significantly reduced SARS-CoV−2 attachment on Calu3 and Caco2 cells by 48% (p = 0.0012) and 55% (p = 0.0445), respectively (Fig. 1d). To further confirm the role of heparan sulfate during SARS-CoV−2 replication, we treated Calu3 and Caco2 cells with heparinases, which contained endoglycosidase activity that cleaved and degraded the polymeric heparan sulfate molecules at the cell surface. In line with the heparan sulfate treatment results, heparinase treatment efficiently reduced SARS-CoV−2 replication in both Calu3 and Caco2 cells (Fig. 1e,f). Specifically, the heparinase I + III treatment reduced SARS-CoV−2 genome copy retrieved from the supernatant of Calu3 and Caco2 cells by 73% (p = 0.0006) and 81% (p = 0.0004), respectively. Next, to evaluate the physiological relevance of heparan sulfate during SARS-CoV−2 infection, we challenged *ex vivo* human lung tissue explants with heparan sulfate- or mock-treated SARS-CoV−2 (Fig. 1g). Our result demonstrated that the heparan sulfate treatment significantly reduced SARS-CoV−2 replication in the tissue homogenate of human lung tissues by 39% (p = 0.0412) (Fig. 1h). In addition to SARS-CoV−2, intervening the interaction between cell surface heparan sulfate and virus particles similarly reduced SARS-CoV attachment and replication (Figure 1a-h), suggesting heparan sulfate played a conserved role during SARS-CoV, SARS-CoV−2, and HCoV-NL63 infection, which all utilized ACE2 for entry. Collectively, our results identified heparan sulfate as an essential attachment receptor for SARS-CoV−2 infection that played an important physiological role for efficient SARS-CoV−2 replication in the human lungs.

Differential role of sialic acids during the attachment and replication of SARS-CoV−2, SARS-CoV, and MERS-CoV

Sialic acid was previously identified to serve as an attachment factor for MERS-CoV [12]. We next investigated if sialic acid could similarly facilitate SARS-CoV−2 attachment and replication. We treated Calu3 and Caco2 cells with neuraminidase (NA) from *Arthrobacter ureafaciens* for 1 hour to remove cell surface sialic acids, followed by virus infection, and quantified virus production in the cell lysates and supernatants at 24 hours post infection. Intriguingly, we observed dramatic differences on the outcome of NA treatment in SARS-CoV−2, SARS-CoV, and MERS-CoV replication. In the lung epithelial Calu3 cells, NA treatment significantly reduced MERS-CoV replication as evidenced by the sharp decrease in virus genome copy in cell lysate and supernatant samples (Fig. 2a), which is in line with previous reports [12,30]. The positive role of sialic acid on MERS-CoV replication was further confirmed with plaque assays, which demonstrated an 86% (p<0.0001) decrease in infectious virus titer upon NA treatment in comparison to the mock-treated samples (Fig. 2a). In stark contrast to MERS-CoV, NA treatment did not decrease but increased SARS-CoV replication. This was confirmed by both qRT-PCR and plaque assays, which showed a 492% (p<0.0001) increase in infectious virus titer upon NA treatment (Fig. 2a). In this regard, our data demonstrated a strictly opposite role of sialic acid on MERS-CoV and SARS-CoV infection, suggesting that while sialic acid facilitated MERS-CoV infection, it served to restrict SARS-CoV infection in Calu3 cells. Next, we evaluated the consequence of NA treatment on SARS-CoV−2 infection. Interestingly, despite a trend of upregulation, NA treatment did not significantly increase SARS-CoV−2 infectious

particle production (p = 0.4942) (Fig. 2a), suggesting that SARS-CoV−2 could partly overcome the sialic acid-mediated restriction in Calu3 cells. The role of sialic acids on virus replication appeared to be cell type specific. In Caco2 cells, while NA treatment did not modulate MERS-CoV replication, it significantly promoted the replication of both SARS-CoV−2 and SARS-CoV (Fig. 2b). In contrast to Calu3 and Caco2 cells, NA treatment did not modulate virus replication for all three viruses in VeroE6 cells (Fig. 2c), which was potentially explained by the difference in the level of cell surface sialic acid expression as suggested from a previous report [12].

To investigate if sialic acid directly impacted the attachment of SARS-CoV−2, SARS-CoV, and MERS-CoV on cell surface, we pretreated Calu3 cells with NA for 1 hour and inoculated the cells with individual viruses at 4 degree for 2 hours (Fig. 2d). Our result demonstrated that while the NA treatment reduced MERS-CoV attachment by 72% (p = 0.0104), it increased SARS-CoV attachment by 39% (p = 0.0189). The attachment of SARS-CoV−2 on Calu3 was marginally increased by NA treatment (10%) and was not significantly different from that of the mock-treated cells (p = 0.7101) (Fig. 2e). In addition, we further evaluated the role of sialic acids on SARS-CoV−2 and SARS-CoV infection with immunofluorescence detection of the viral nucleocapsid (N) protein. The imaging results indicated that while NA treatment modestly increased SARS-CoV−2 infection in Calu3, the increase was more evident for SARS-CoV. In Caco2 cells, NA treatment efficiently promoted the infection of both viruses (Fig. 2f).

The differential interplay with sialic acids during SARS-CoV−2 and SARS-CoV infection is potentially important and may contribute to the difference in the efficiency of infecting and replicating in human lung cells by the two viruses [31,32]. To further investigate the interaction of SARS-CoV−2 and SARS-CoV with sialic acids, we employed the solute carrier family 35 member A1 (SLC35A1) knockout HEK293 cells, which are deficient in cell surface sialic acid expression and are resistant to influenza virus infection (Fig. 3a and Supplementary Fig. 1) [33]. With ACE2 overexpression (Fig. 3b), the attachment of SARS-CoV on the cell surface of the control knockout cells (SLC35A1^{WT}/ACE2^{oe}) was 868% than that of the mock-overexpressed cells (SLC35A1^{WT}/ACE2^{m}). In ACE2-overexpressed SLC35A1 knockout cells (SLC35A1^{KO}/ACE2^{oe}), SARS-CoV attachment significantly further increased to 1423% in comparison to the control (SLC35A1^{WT}/ACE2^{m}) (SARS-CoV/SLC35A1^{KO}/ACE2^{oe} vs SARS-CoV/SLC35A1^{WT}/ACE2^{oe}: p<0.0001) (Fig. 3c). However, the attachment of SARS-CoV−2 was only modestly increased in the surface sialic acid deficient cells (SLC35A1^{KO}/ACE2^{oe}: 846%) in comparison to the control (SLC35A1^{WT}/ACE2^{oe}: 723%) (SARS-CoV−2/SLC35A1^{KO}/ACE2^{oe} vs SARS-CoV−2/SLC35A1^{WT}/ACE2^{oe}: p = 0.4914) (Fig. 3c).

To investigate whether sialic acids played physiologically important roles during SARS-CoV−2 and SARS-CoV infection of the human lungs, we treated *ex vivo* human lung tissues with NA, followed by SARS-CoV−2 or SARS-CoV challenge. Our results showed that SARS-CoV−2 replicated more efficiently than SARS-CoV in the human lung without NA treatment (p = 0.0077 at 48 hpi) (Fig. 3d), which was consistent with our previous report [31]. The NA treatment significantly increased the replication of SARS-CoV (p = 0.0048 at 48 hpi) but not SARS-CoV−2 (p = 0.1173 at 48 hpi) in the human lung tissues, which mitigated the replication difference between SARS-CoV−2 and SARS-CoV (p = 0.1713 at 48hpi) (Fig. 3d). The more

sizable increase for SARS-CoV over SARS-CoV−2 replication upon NA treatment was additionally evidenced by the significant increase in intracellular virus genome copies and infectious virus titers in SARS-CoV but not SARS-CoV−2 infection (Fig. 3e,f). We next performed immunohistochemistry to directly visualize the effect of NA treatment on SARS-CoV−2 and SARS-CoV infection in the human lung tissues. As demonstrated in Fig. 3g, while NA treatment dramatically increased the extent of SARS-CoV infection (middle panels, arrows) in human lung tissues, the level of SARS-CoV−2 infection was modestly affected (left panels). Taken together, our results demonstrated an unexpected role of sialic acids in restricting SARS-CoV−2 and SARS-CoV replication in human lung tissues. More importantly, the capacity of SARS-CoV−2 in overcoming the sialic acid-mediated restriction might contribute to the highly efficient infection and replication of SARS-CoV−2 in human lungs.

The inserted furin-like cleavage site in the SARS-CoV−2 spike is required for efficient virus replication in the human lung

Recent studies identified a four amino acid insertion at the boundary between the SARS-CoV−2 spike S_1 and S_2 subunits [23,24], resulting in a "RRAR" furin-like cleavage site in SARS-CoV−2 spike. These residues are not present at the S_1/S_2 cleavage site of SARS-CoV spike, SARSr-CoV spike, and the closely related bat coronavirus RaTG13 spike [25]. Similar amino acid insertions that created a polybasic furin cleavage site were reported in the hemagglutinin protein of influenza viruses and were found to contribute to virus virulence [34]. However, the physiological importance of this furin-like cleavage site introduced at S_1/S_2 junction of SARS-CoV−2 spike has not been functionally evaluated during virus infection. To this end, we first overexpressed human furin and ACE2 in the non-permissive BHK21 cells (Fig. 4a), followed by SARS-CoV−2 or SARS-CoV infection, and assessed virus replication at 24 hpi. Interestingly, SARS-CoV−2 replicated to similar levels in the ACE2^{oe}/Furin^{oe} and the ACE2^{oe}/Furin^m BHK21 cells (Fig. 4b,c), suggesting that the expression of furin did not facilitate SARS-CoV−2 replication in the ACE2-expressing BHK21 cells. Next, we compared the replication of SARS-CoV−2 with a SARS-CoV−2 mutant (SARS-CoV−2 S_1/S_2mut), which contained a 10-amino acid deletion in spike that removed the S_1/S_2 furin-like cleavage site (Fig. 4d and supplementary Fig. 2) in Huh7 cells with or without furin overexpression (Fig. 4e). Our data demonstrated that SARS-CoV−2 S_1/S_2mut and SARS-CoV−2 replicated to largely comparable levels in Huh7 cells (Fig. 4f,g). At the same time, overexpression of furin in Huh7 did not promote the replication of SARS-CoV−2 S_1/S_2mut or SARS-CoV−2 (Fig. 4f,g).

Next, we infected a panel of seven different cell types of human and non-human origin, including Caco2 (human intestine), Calu3 (human lung), Huh7 (human liver), CRFK (cat), RK13 (rabbit), PK15 (pig), and VeroE6 (monkey) cells, with SARS-CoV−2 or SARS-CoV−2 S_1/S_2mut. Interestingly, SARS-CoV−2 replicated significantly better than SARS-CoV−2 S_1/S_2mut in Calu3 (25.2-folds; p = 0.0046) but not the other evaluated cells (Fig. 5a). To understand why the furin cleavage site was required for efficient SARS-

CoV−2 replication in Calu3 but not other cells, we analysed the expression level of ACE2 and representative host proteases from three representative permissive human cells (Caco2, Calu3, Huh7) as well as three representative human cells that did not support SARS-CoV−2 replication (A549, HFL, RD) [32]. Our results suggested that Caco2 cells expressed the highest level of TMPRSS2, which was 46- and 28-folds higher than that of Calu3 and Huh7, respectively. At the same time, Huh7 cells expressed the highest level of cathepsin L, which was 19- and 14-folds higher than that of Caco2 and Calu3, respectively (Fig. 5b). Calu3 expressed low levels of both TMPRSS2 and cathepsin L, which were the representative enzyme responsible for plasma membrane and endosomal entry, respectively (Fig. 5b). These findings suggested that in model cell lines, furin cleavage at S_1/S_2 junction of spikewas required for efficient SARS-CoV−2 replication in the absence of either a robust plasma membrane entry pathway or a robust endosomal entry pathway.

We next compared the replication of SARS-CoV−2 and SARS-CoV−2 S_1/S_2mut in *ex vivo* human lung tissues and *ex vivo* human intestine tissues (Fig. 5c). Importantly, SARS-CoV−2 replicated more efficiently than that of SARS-CoV−2 S_1/S_2mut in the human lung tissues (Fig. 5d,e). Specifically, SARS-CoV−2 replicated 3.2-fold (p = 0.0042) and 2.3-fold (p = 0.0011) higher than that of SARS-CoV−2 S_1/S_2mut at 36 and 60 hpi, respectively (Fig. 5d). Interestingly, despite their differential replication capacity in human lung tissues, the two viruses replicated to similar levels in *ex vivo* human intestine tissues (Fig. 5f,g). Next, we evaluated the expression of ACE2 and representative proteases in human lung and intestine tissues. Our results revealed that the TMRPSS2 expression level in the human intestine tissues was 13-folds higher than that in the human lung tissues, which might explain the dependency on furin activation of the viral spike protein for SARS-CoV−2 replication in the human lung but not intestine (Fig. 5h). Overall, these results suggested that the inserted furin-like cleavage site located at the S_1/S_2 junction of SARS-CoV−2 spike is required for efficient virus replication in the human lungs.

Discussion

As evidenced by the rapid dissemination of SARS-CoV−2 globally, this novel betacoronavirus is highly efficient in person-to-person transmission [5,6]. Understanding the host and viral determinants that contribute to efficient SARS-CoV−2 infection of human cells could provide insights on the biology of SARS-CoV−2 transmission and pathogenesis, and potentially reveal targets of intervention. In this study, we described key host and viral features that contributed to the efficient replication of SARS-CoV−2 in the human lungs, which were not previously reported (Fig. 6). First, we identified heparan sulfate as an attachment receptor for SARS-CoV−2 infection in *in vitro* human lung epithelial cells and *ex vivo* human lung tissue explants. Second, we identified sialic acid as a host factor that restricted SARS-CoV−2 and SARS-CoV infection. More importantly, SARS-CoV−2 was capable of overcoming the sialic acid-mediated restriction, which facilitated its replication in the human lung tissues. Third, we identified the furin-like cleavage site at the S_1/S_2 junction of SARS-CoV−2 spike to be essential for efficient virus replication in human lung epithelial cells. We further showed that SARS-CoV−2 replicated to significantly higher levels in the *ex vivo* human lung tissues than that of SARS-CoV−2 S_1/S_2mut. The difference was organ-specific

as the replication of the two viruses was comparable in *ex vivo* human intestine tissues. By analyzing the expression of host factors for SARS-CoV−2 entry in human lung and intestine tissues, our results suggested that the dependency on furin cleavage of spike for efficient SARS-CoV−2 replication in the human lung was due to a relatively low level of TMPRSS2 expression. Collectively, our study revealed critical host and viral determinants for efficient SARS-CoV−2 replication in the human lung, which extended our understanding on the biology of SARS-CoV−2 infection and transmission.

Heparan sulfate is a linear polysaccharide that contains N-acetylglucosamine (GlcNAc) and glucuronic acid (GlcA), with groups of sulfate and other modifications [35]. It serves as a major adhesion receptor for a large number of viruses including human immunodeficiency virus, respiratory syncytial virus, and dengue virus [36−38]. In addition, heparan sulfate also functions as an entry receptor for herpes simplex virus type 1 [39]. In the context of human coronavirus, heparan sulfate was previously reported to serve as an indispensable attachment receptor for HCoV-NL63 [11]. By blocking the interaction between cell surface heparan sulfate and virus spike, the attachment and infection of HCoV-NL63 was largely abolished [11]. Here, we demonstrated that blocking the interaction between cell surface heparan sulfate and virus spike with exogenous heparan sulfate pretreatment significantly reduced SARS-CoV−2 attachment on Calu3 cells by 48% (p = 0.0012). Meanwhile, removing cell surface heparan sulfate by heparinase treatment reduced SARS-CoV−2 in the supernatant of Calu3 cells by 73% (p = 0.0006) at 24 hpi. These evidence suggested an essential role of heparan sulfate in SARS-CoV−2 attachment and replication. Since heparan sulfate is ubiquitously expressed by most cell types, it may serve an important role during SARS-CoV−2 infection as ACE2 expression is relatively low in the lung and respiratory tract comparing to many other human tissues [18]. In this regard, blocking the interaction between cell surface heparan sulfate and viral spike should be considered as a potential intervention strategy for COVID−19. Interestingly, as a common anticoagulant, heparin was applied in the treatment of COVID−19 coagulopathy and was found to associate with decreased mortality in severe cases [40]. Since heparin is structurally similar with that of heparan sulfate, its potential capacity on blocking SARS-CoV−2 infection should be further explored.

Sialic acid was a recognized host factor that served as an attachment factor or entry receptor for a number of coronaviruses including transmissible gastroenteritis virus (TGEV), bovine coronavirus (BCoV), HCoV-OC43, and HCoV-HKU1 [13,14,41,42]. Recently, MERS-CoV spike was identified to have sialic acid binding capacity and sialic acid depletion in Calu3 cells reduced MERS-CoV entry by more than 70% compared with mock-treatment [12]. However, the role of sialic acid in SARS-CoV−2 or SARS-CoV infection is unknown. Here, by using a combination of human lung epithelial cells, SLC35A1^{KO} cells, and *ex vivo* human lung tissues, we demonstrated an unexpected role of cell surface sialic acid against SARS-CoV infection. In comparison to SARS-CoV, SARS-CoV−2 attachment and replication was less restricted by cell surface sialic acids. This might be explained by the higher ACE2 binding affinity by SARS-CoV−2 receptor-binding domain (RBD) comparing to SARS-CoV RBD [43,44]. Since sialic acids are abundantly expressed in the human respiratory tract, the capacity of SARS-CoV−2 to overcome sialic acid-mediated restriction in comparison to SARS-CoV may contribute to its efficient replication and person to person transmission. Interestingly, to promote virus replication, influenza viruses encode for viral neuraminidase

for efficient virus release from the infected host cells. In addition, a number of bacteria also express sialidase [45]. In this regard, the modulatory effect of influenza viruses and bacteria on SARS-CoV−2 infection might deserve further investigations.

The "PRRA" amino acid insertion at the S_1/S_2 junction of SARS-CoV−2 spike was recently identified and was widely speculated to facilitate virus replication or expand virus tropism [23,24,26]. In this study, we carefully evaluated the importance of the reported S_1/S_2 furin cleavage site in SARS-CoV−2 spike during SARS-CoV−2 infection. Interestingly, SARS-CoV−2 replicated better than SARS-CoV−2 S_1/S_2mut in the human lung epithelial cells (Calu3), which expressed low levels of TMPRSS2 and cathepsin L. Since TMPRSS2 and cathepsin L are the representative proteases responsible for plasma membrane and endosomal entry pathways, respectively, our findings indicated that furin cleavage of the virus spike would be essential for efficient SARS-CoV−2 replication in cell lines without either a robustly operative plasma membrane or endosomal entry pathway. Previous studies suggested that human coronaviruses could utilize either the plasma membrane serine protease TMPRSS2 or endosomal cysteine proteases cathepsin L for spike activation and virus entry in cell lines [20−22]. However, TMPRSS2 played a more predominant role in virus replication and infection than cathepsin L in primary cells and animal models [46−48]. In line with this finding, we further demonstrated that furin cleavage at S_1/S_2 junction of SARS-CoV−2 spike was required for efficient SARS-CoV−2 replication in the human lung but not intestine, potentially due to the significantly lower TMPRSS2 expression in the lung comparing to the intestine. In this regard, the potential of TMPRSS2 and furin inhibition should be further explored as potential intervention strategies against SARS-CoV−2 since the respiratory tract is the primary target of the virus.

In summary, our study revealed essential host and viral determinants for SARS-CoV−2 infection of the human lung. These findings contributed to our understanding on the efficient replication of SARS-CoV−2 in the respiratory tract and suggested targets of intervention against COVID−19.

Methods

Viruses and biosafety

SARS-CoV−2 HKU−001a (GenBank accession number MT230904) was isolated from the nasopharyngeal aspirate of a laboratory-confirmed COVID−19 patient in Hong Kong as previously described [32]. SARS-CoV GZ50 (GenBank accession number AY304495) was an archived clinical isolate at Department of Microbiology, HKU. MERS-CoV EMC/2012 was kindly provided by Dr Ron Fouchier from Erasmus Medical Center. The influenza A virus strain A/Hong Kong/415742/2009(H1N1)pdm09 was isolated and archived at Department of Microbiology, HKU [49]. VeroE6 cells were used to culture SARS-CoV−2, SARS-CoV, and MERS-CoV. H1N1 were cultured in chicken embryo. All viruses were titrated by plaque assays. SARS-CoV−2 HKU−001a S_1/S_2mut (GenBank accession numberMT621560), which carried a 10 amino acid deletion, was isolated by plaque purification from SARS-CoV−2 cultured in VeroE6 cells and subsequently sequenced (Supplementary Fig. 2). All experiments with infectious SARS-

CoV−2, SARS-CoV−2 S$_1$/S$_2$mut, SARS-CoV, and MERS-CoV were performed following the approved standard operating procedures of the Biosafety Level 3 facility at Department of Microbiology, HKU.

Cell cultures

Calu3, Caco2, Huh7, BHK21, RD, A549, RK13, PK15, CRFK, and VeroE6 were obtained from ATCC. The HFL cells were developed in-house. The cells were maintained in minimum essential medium (MEM) (Gibco, MA, USA), Dulbecco's modified Eagle's medium (DMEM) (Gibco), or DMEM/F12 (Gibco) according to supplier's instructions. The cell lines used are routinely tested for mycoplasma and are maintained mycoplasma-free.

Human *ex vivo* lung and intestine tissues and virus inoculation on tissues

Human lung and intestine tissues in our *ex vivo* studies were acquired from patients undergoing surgeries at Queen Mary Hospital, Hong Kong as we previously described [31]. All donors provided written consent as approved by the Institutional Review Board of the University of Hong Kong/Hospital Authority Hong Kong West Cluster. The tissues were maintained and processed freshly immediately upon receipt, as we described previously [31]. The processed specimens were infected with SARS-CoV, SARS-CoV−2, or SARS-CoV−2 S$_1$/S$_2$mut at an inoculum of 1×10^7PFU/ml per well.

Heparan sulfate and heparinase treatment

Heparan sulfate (HS) (HY−101916, MedChemExpress, NJ, USA) was incubated with viruses before infection at the indicated concentrations at room temperature for 1h. For virus attachment assays, the pretreated viruses were incubated with cells at 0.2MOI at 4°C for 2h, washed, and harvested. For replication assays, the pretreated viruses were incubated with cells at 0.2MOI at 37°C for 2h. The cells were washed after 2h and incubated in HS-supplemented culture media. Cell lysates and supernatants were harvested at 24 hpi. For heparinase assays, Calu3 or Caco2 cells were pretreated with Heparinase I (4U/ml) (P0735L, NEB, MA, USA), Heparinase III (0.5U/ml) (P0737L, NEB), or both at 37 °C for 1h. Viruses were inoculated into the pretreated cells at 0.2MOI for 2h at 37°C. Cell lysates and supernatants were harvested at 24 hpi. For HS treatment on *ex vivo* human lung tissues, SARS-CoV−2 and SARS-CoV at 1×10^7PFU/ml were pre-incubated with 1000μg/ml HS for 1h at room temperature. Lung tissues were inoculated with pretreated viruses for 2h, washed, incubated in HS-supplemented culture media, and harvested at 24hpi.

Neuraminidase treatment on cell lines and *ex vivo* human lung tissues

To determine the role of sialic acids during SARS-CoV−2 and SARS-CoV infection in cell lines, Caco2 and Calu3 cells were pretreated with 12.5U neuraminidase A (NA) from *Arthrobacter ureafaciens* (P0722L, NEB) at 37 °C for 1h before infection. The pretreated cells were challenged with SARS-CoV−2 or SARS-CoV at 0.2MOI for 2h at 4°C for virus attachment assays. Alternatively, the pretreated cells were challenged with SARS-CoV−2 or SARS-CoV at 0.2MOI for 2h at 37°C for virus replication assays. At 2hpi, the cells were washed and NA-supplemented culture media were added. Cell lysates and supernatants were collected at 24 hpi. For *ex vivo* human lung tissues, the lung specimens were pre-incubated with 50U NA for 1h at 37 °C. Pretreated human lung tissues were challenged with SARS-CoV−2 and SARS-CoV at $1x10^7$PFU/ml for 2h. After virus inoculation, the lung tissues were washed, incubated in NA-supplemented culture media, and harvested at the indicated time points.

Sialic acid transporter SLC35A1 knockout cells

SLC35A1 sgRNA oligos (5′—CACCGCCATAGCTTTAAGATACACA—3′ and 3′—CGGTATCGAAATTCTATGTGTCAAA—5′) were annealed by heating to 95°C for 5 minutes and cooling to 25°C at 1.5°C/minute. The lentiCRISPR v2 plasmid (Addgene) was digested by BsmBI (NEB) and purified by electrophoresis and gel purification. The digested lentiCRISPR v2 plasmid (Addgene) and annealed oligos were then ligated into SLC35A1-lentiCRISPR using the Quick Ligation Kit (M2200L, NEB). Ligation products were purified by the PureLink PCR purification kit (Thermo Fisher Scientific, MA, USA). Purified plasmids were transformed into DH5α competent cells and selected with ampicillin. At 14 hours after transformation, colonies were picked for sequence analysis using human U6 primer. Positive colonies were expanded and extracted using QIAGEN Plasmid Plus Kits (12963, QIAGEN, Hilden, Germany) to obtain the SLC35A1-lentiCRISPR plasmid. The SLC35A1-lentiCRISPR plasmid was co-transfected with packaging plasmids pMD2.G (Addgene) and psPAX2 (Addgene) into 293T cells using Lipofectamine 3000 (L3000015, Thermo Fisher Scientific). The cell supernatant that contained SLC35A1-lentiCRISPR lentiviruses was harvested at 48 hpi and used for transduction. The transduced HEK293 cells were selected for 72 hours in 1µg/ml puromycin and were limiting diluted in 96-well plates for clonal expansion. Depletion of SLC35A1 expression in these clones was determined by DNA sequencing. The phenotype of SLC35A1 knockout was confirmed by immunofluorescence staining for cell surface sialic acids with Sambucus Nigra (SNA) lectin (FL−1301, Vector Laboratories, CA, USA). In addition, the SLC35A1 knockout cells were functional evaluated by loss of capacity of supporting influenza virus H1N1 infection. For this purpose, SLC35A1 or control knockout cells were challenged with H1N1 at 0.1 MOI for 1 hour at 37 °C. At 24 hours post virus challenge, the cell lysates were harvested for qRT-PCR analysis of virus replication. To evaluate the role of sialic acid on SARS-CoV−2 or SARS-CoV attachment, SLC35A1- and control-knockout HEK293 cells were transfected with hACE2 plasmid or empty vector for 24h. The transfected cells were challenged with SARS-CoV−2 or SARS-CoV at 0.2 MOI for 2h at 4°C. After

2 hours, the inoculum was removed and the cells were washed 3 times with PBS. Cell lysates were harvested in RLT buffer (Qiagen) for qRT-PCR analysis.

RNA extraction and qRT-PCR

RNA extraction and qRT-PCR were performed as we previously described [50,51]. Cell lysates and tissue samples were lysed by RLT buffer (Qiagen) and extracted with the RNeasy Mini kit (74106, Qiagen). Supernatant samples were lysed by AVL buffer (Qiagen) and extracted with the QIAamp Viral RNA Mini kit (52906, Qiagen). After RNA extraction, qRT-PCR was performed using the QuantiNova SYBR Green RT-PCR kit (208154, Qiagen) or the QuantiNova Probe RT-PCR Kit (208354, Qiagen) with the LightCycler 480 Real-Time PCR System (Roche, Basel, Switzerland). The primer and probe sequences were previous described [32,52].

Plaque assay

VeroE6 cells were seeded in 12-well plates one day before the experiment. The harvested supernatant samples were serially diluted and inoculated to the cells for 2h at 37°C. After inoculation, the cells were washed with PBS 3 times, and covered with 2% agarose/PBS mixed with 2X DMEM / 2%FBS at 1:1 ratio. The cells were fixed after incubation at 37°C for 72h. Fixed samples were stained with 0.5% crystal violet in 25% ethanol/distilled water for 10min for plaque visualization.

Immunofluorescence staining

Immunofluorescence staining was performed as we previously described with slight modifications [53]. Briefly, infected cells were fixed overnight in 10% formalin. The fixed samples were washed with PBS and blocked by serum-free protein blocker (X0909, Dako, Glostrup, Denmark) and Sudan black B. The samples were then stained with an in-house rabbit anti-SARS-CoV–2-nucleocapsid (N) immune serum or an in-house rabbit anti-SARS-CoV-N immune serum for virus detection. Sambucus Nigra lectin (SNA) from Vector Laboratories was used for sialic acid detection. Goat anti-rabbit IgG secondary antibody (O–11038) was purchased from Thermo Fisher Scientific. The antifade mounting medium with DAPI (H–1200, Vector Laboratories) was used for mounting and DAPI staining. Images were taken with the Olympus BX53 fluorescence microscope (Olympus Life Science, Tokyo, Japan).

Immunohistochemistry

Immunohistochemistry was performed as we previously described with slight modifications [31]. Human lung tissue samples were collected and fixed overnight in 10% formalin. The fixed samples were embedded in paraffin by TP1020 Leica semi-enclosed benchtop tissue processor and sectioned with

microtome (Thermo Fisher Scientific). Sectioned samples were prepared on glass slides and were dewaxed and dehydrated by serially diluted xylene, ethanol, and double-distilled water in sequence. Afterwards, the samples were co-heated together with antigen unmasking solution (H−3300, Vector Laboratories) at 85 °C for 90s for antigen exposure, followed by blocking with 0.3% hydrogen peroxide for 30min, and 1% BSA for 30min. The in-house rabbit anti-SARS-CoV−2-N immune serum or in-house rabbit anti-SARS-CoV-N immune serum were applied as the primary antibodies and were incubated with the slides at 4 °C overnight. The signal was developed with the DAB (3,3'-diaminobenzidine) substrate kit (SK−4100, Vector Laboratories). Cell nuclei were labeled with Gill's haematoxylin. The slides were mounted with antifade mounting medium with DAPI (H−1200, Vector Laboratories). Images were taken with the Olympus BX53 light microscope (Olympus Life Science).

Western blot

Cells grown on 24-well plate were transfected with furin-flag and/or hACE2-V5 plasmids using Lipofectamine 3000 (Thermo Fisher Scientific). Cells were lysed by RIPA buffer (89901, Thermo Fisher Scientific) with protease inhibitor (4693159001, Roche, Basel, Switzerland) at 24h post transfection. Proteins were separated with SDS-PAGE and transferred to nitrocellulose membrane. Specific primary antibodies were incubated with the blocked membranes at 4°C overnight, followed by horseradish peroxidase (HRP) conjugated secondary antibodies (Thermo Fisher Scientific) for 1h at room temperature. The signal was developed by Immobilon Crescendo Western HRP Substrate (WBLUR0500, Merck Millipore, MA, USA) and detected using Alliance Imager apparatus (Uvitec, Cambridge, UK). Rabbit anti-human furin antibody (ab183495, Abcam, Cambridge, UK) was used as the primary antibody for furin detection. Human ACE2 was detected with a rabbit anti-V5 antibody (CM3005, ImmunoWay, TX, USA). Beta-actin was used as the loading control, which was detected by mouse anti-human beta-actin antibody (MAB8929, R&D).

Statistical analysis

Data represented mean and standard deviations. Statistical differences between two groups were evaluated with Student's t-test using GraphPad Prism 6. Statistical differences between three or more groups were evaluated with two-way ANOVA using Graphpad Prism 6. Differences were considered statistically significant when $P < 0.05$.

Declarations

Author contributions

HC, JFWC, and KYY designed the study. HC, BH, XH, YC, YW, HS, DY, YH, XZ, TTTY, JPC, AJZ, JZ, SY, KKWT, IHYC, KYS, DCCF, IYHW, ATLN, TTC, SYKL, WKA, and KHK performed experiments, analyzed data, or provided key resources. HC, JFWC, and KYY wrote the manuscript.

Competing interests

The authors declare no competing interests.

Materials and correspondence

Correspondence and material requests should be addressed to Prof Kwok-Yung Yuen and Dr. Jasper Fuk-Woo Chan.

Data availability

The data that support the findings of this study are available from the corresponding authors upon reasonable request.

References

1   Zhu, N. *et al.* A Novel Coronavirus from Patients with Pneumonia in China, 2019. *N Engl J Med*, doi:10.1056/NEJMoa2001017 (2020).

2   Cheng, V. C., Lau, S. K., Woo, P. C. & Yuen, K. Y. Severe acute respiratory syndrome coronavirus as an agent of emerging and reemerging infection. *Clin Microbiol Rev* **20**, 660-694, doi:10.1128/CMR.00023-07 (2007).

3   Guan, W. J. *et al.* Clinical Characteristics of Coronavirus Disease 2019 in China. *N Engl J Med*, doi:10.1056/NEJMoa2002032 (2020).

4   Chan, J. F. *et al.* Genomic characterization of the 2019 novel human-pathogenic coronavirus isolated from a patient with atypical pneumonia after visiting Wuhan. *Emerg Microbes Infect* **9**, 221-236, doi:10.1080/22221751.2020.1719902 (2020).

5   Chan, J. F. *et al.* A familial cluster of pneumonia associated with the 2019 novel coronavirus indicating person-to-person transmission: a study of a family cluster. *Lancet*, doi:10.1016/S0140-6736(20)30154-9 (2020).

6   WHO. Coronavirus disease (COVID-19) Situation Report – 150 (2020).

7   Hofmann, H. & Pohlmann, S. Cellular entry of the SARS coronavirus. *Trends Microbiol* **12**, 466-472, doi:10.1016/j.tim.2004.08.008 (2004).

8   Li, F. Structure, Function, and Evolution of Coronavirus Spike Proteins. *Annu Rev Virol* **3**, 237-261, doi:10.1146/annurev-virology-110615-042301 (2016).

9   Chan, C. M. *et al.* Carcinoembryonic Antigen-Related Cell Adhesion Molecule 5 Is an Important Surface Attachment Factor That Facilitates Entry of Middle East Respiratory Syndrome Coronavirus. *J Virol* **90**, 9114-9127, doi:10.1128/JVI.01133-16 (2016).

10   Chu, H. *et al.* Middle East respiratory syndrome coronavirus and bat coronavirus HKU9 both can utilize GRP78 for attachment onto host cells. *J Biol Chem* **293**, 11709-11726, doi:10.1074/jbc.RA118.001897 (2018).

11   Milewska, A. *et al.* Human coronavirus NL63 utilizes heparan sulfate proteoglycans for attachment to target cells. *J Virol* **88**, 13221-13230, doi:10.1128/JVI.02078-14 (2014).

12   Li, W. *et al.* Identification of sialic acid-binding function for the Middle East respiratory syndrome coronavirus spike glycoprotein. *Proc Natl Acad Sci U S A* **114**, E8508-E8517, doi:10.1073/pnas.1712592114 (2017).

13   Huang, X. *et al.* Human Coronavirus HKU1 Spike Protein Uses O-Acetylated Sialic Acid as an Attachment Receptor Determinant and Employs Hemagglutinin-Esterase Protein as a Receptor-Destroying Enzyme. *J Virol* **89**, 7202-7213, doi:10.1128/JVI.00854-15 (2015).

14   Krempl, C., Schultze, B. & Herrler, G. Analysis of cellular receptors for human coronavirus OC43. *Adv Exp Med Biol* **380**, 371-374, doi:10.1007/978-1-4615-1899-0_60 (1995).

15   Watanabe, R., Sawicki, S. G. & Taguchi, F. Heparan sulfate is a binding molecule but not a receptor for CEACAM1-independent infection of murine coronavirus. *Virology* **366**, 16-22, doi:10.1016/j.virol.2007.06.034 (2007).

16   Hoffmann, M. *et al.* SARS-CoV-2 Cell Entry Depends on ACE2 and TMPRSS2 and Is Blocked by a Clinically Proven Protease Inhibitor. *Cell* **181**, 271-280 e278, doi:10.1016/j.cell.2020.02.052 (2020).

17   Zhou, P. *et al.* A pneumonia outbreak associated with a new coronavirus of probable bat origin. *Nature*, doi:10.1038/s41586-020-2012-7 (2020).

18   Venkatakrishnan, A. J. *et al.* Knowledge synthesis of 100 million biomedical documents augments the deep expression profiling of coronavirus receptors. *Elife* **9**, doi:10.7554/eLife.58040 (2020).

19   Millet, J. K. & Whittaker, G. R. Host cell entry of Middle East respiratory syndrome coronavirus after two-step, furin-mediated activation of the spike protein. *Proc Natl Acad Sci U S A* **111**, 15214-15219, doi:10.1073/pnas.1407087111 (2014).

20   Shirato, K., Kawase, M. & Matsuyama, S. Middle East respiratory syndrome coronavirus infection mediated by the transmembrane serine protease TMPRSS2. *J Virol* **87**, 12552-12561, doi:10.1128/JVI.01890-13 (2013).

21   Shulla, A. *et al.* A transmembrane serine protease is linked to the severe acute respiratory syndrome coronavirus receptor and activates virus entry. *J Virol* **85**, 873-882, doi:10.1128/JVI.02062-10 (2011).

22   Simmons, G. *et al.* Inhibitors of cathepsin L prevent severe acute respiratory syndrome coronavirus entry. *Proc Natl Acad Sci U S A* **102**, 11876-11881, doi:10.1073/pnas.0505577102 (2005).

23   Coutard, B. *et al.* The spike glycoprotein of the new coronavirus 2019-nCoV contains a furin-like cleavage site absent in CoV of the same clade. *Antiviral Res* **176**, 104742, doi:10.1016/j.antiviral.2020.104742 (2020).

24   Walls, A. C. *et al.* Structure, Function, and Antigenicity of the SARS-CoV-2 Spike Glycoprotein. *Cell* **181**, 281-292 e286, doi:10.1016/j.cell.2020.02.058 (2020).

25   Andersen, K. G., Rambaut, A., Lipkin, W. I., Holmes, E. C. & Garry, R. F. The proximal origin of SARS-CoV-2. *Nat Med* **26**, 450-452, doi:10.1038/s41591-020-0820-9 (2020).

26   Hoffmann, M., Kleine-Weber, H. & Pohlmann, S. A Multibasic Cleavage Site in the Spike Protein of SARS-CoV-2 Is Essential for Infection of Human Lung Cells. *Mol Cell* **78**, 779-784 e775, doi:10.1016/j.molcel.2020.04.022 (2020).

27   Lamers, M. M. *et al.* SARS-CoV-2 productively infects human gut enterocytes. *Science*, doi:10.1126/science.abc1669 (2020).

28   Wang, X. *et al.* SARS-CoV-2 infects T lymphocytes through its spike protein-mediated membrane fusion. *Cell Mol Immunol*, doi:10.1038/s41423-020-0424-9 (2020).

29   Milewska, A. *et al.* Entry of Human Coronavirus NL63 into the Cell. *J Virol* **92**, doi:10.1128/JVI.01933-17 (2018).

30   Park, Y. J. *et al.* Structures of MERS-CoV spike glycoprotein in complex with sialoside attachment receptors. *Nat Struct Mol Biol* **26**, 1151-1157, doi:10.1038/s41594-019-0334-7 (2019).

31   Chu, H. *et al.* Comparative replication and immune activation profiles of SARS-CoV-2 and SARS-CoV in human lungs: an ex vivo study with implications for the pathogenesis of COVID-19. *Clin Infect Dis*, doi:10.1093/cid/ciaa410 (2020).

32   Chu, H. *et al.* Comparative tropism, replication kinetics, and cell damage profiling of SARS-CoV-2 and SARS-CoV with implications for clinical manifestations, transmissibility, and laboratory studies of COVID-19: an observational study. *Lancet Microbe*, doi:https://doi.org/10.1016/S2666-5247(20)30004-5 (2020).

33   Han, J. *et al.* Genome-wide CRISPR/Cas9 Screen Identifies Host Factors Essential for Influenza Virus Replication. *Cell Rep* **23**, 596-607, doi:10.1016/j.celrep.2018.03.045 (2018).

34   Claas, E. C. *et al.* Human influenza A H5N1 virus related to a highly pathogenic avian influenza virus. *Lancet* **351**, 472-477, doi:10.1016/S0140-6736(97)11212-0 (1998).

35   Sarrazin, S., Lamanna, W. C. & Esko, J. D. Heparan sulfate proteoglycans. *Cold Spring Harb Perspect Biol* **3**, doi:10.1101/cshperspect.a004952 (2011).

36   Roderiquez, G. *et al.* Mediation of human immunodeficiency virus type 1 binding by interaction of cell surface heparan sulfate proteoglycans with the V3 region of envelope gp120-gp41. *J Virol* **69**, 2233-2239 (1995).

37   Feldman, S. A., Audet, S. & Beeler, J. A. The fusion glycoprotein of human respiratory syncytial virus facilitates virus attachment and infectivity via an interaction with cellular heparan sulfate. *J Virol* **74**, 6442-6447, doi:10.1128/jvi.74.14.6442-6447.2000 (2000).

38   Chen, Y. *et al.* Dengue virus infectivity depends on envelope protein binding to target cell heparan sulfate. *Nat Med* **3**, 866-871, doi:10.1038/nm0897-866 (1997).

39   Shukla, D. *et al.* A novel role for 3-O-sulfated heparan sulfate in herpes simplex virus 1 entry. *Cell* **99**, 13-22, doi:10.1016/s0092-8674(00)80058-6 (1999).

40   Tang, N. *et al.* Anticoagulant treatment is associated with decreased mortality in severe coronavirus disease 2019 patients with coagulopathy. *J Thromb Haemost* **18**, 1094-1099, doi:10.1111/jth.14817 (2020).

41   Schultze, B. *et al.* Transmissible gastroenteritis coronavirus, but not the related porcine respiratory coronavirus, has a sialic acid (N-glycolylneuraminic acid) binding activity. *J Virol* **70**, 5634-5637 (1996).

42   Schultze, B., Gross, H. J., Brossmer, R. & Herrler, G. The S protein of bovine coronavirus is a hemagglutinin recognizing 9-O-acetylated sialic acid as a receptor determinant. *J Virol* **65**, 6232-6237 (1991).

43   Shang, J. *et al.* Cell entry mechanisms of SARS-CoV-2. *Proc Natl Acad Sci U S A* **117**, 11727-11734, doi:10.1073/pnas.2003138117 (2020).

44   Shang, J. *et al.* Structural basis of receptor recognition by SARS-CoV-2. *Nature* **581**, 221-224, doi:10.1038/s41586-020-2179-y (2020).

45   Vimr, E. R., Kalivoda, K. A., Deszo, E. L. & Steenbergen, S. M. Diversity of microbial sialic acid metabolism. *Microbiol Mol Biol Rev* **68**, 132-153, doi:10.1128/mmbr.68.1.132-153.2004 (2004).

46   Zhou, Y. *et al.* Protease inhibitors targeting coronavirus and filovirus entry. *Antiviral Res* **116**, 76-84, doi:10.1016/j.antiviral.2015.01.011 (2015).

47   Simmons, G. *et al.* Different host cell proteases activate the SARS-coronavirus spike-protein for cell-cell and virus-cell fusion. *Virology* **413**, 265-274, doi:10.1016/j.virol.2011.02.020 (2011).

48   Iwata-Yoshikawa, N. *et al.* TMPRSS2 Contributes to Virus Spread and Immunopathology in the Airways of Murine Models after Coronavirus Infection. *J Virol* **93**, doi:10.1128/JVI.01815-18 (2019).

49   Yuan, S. *et al.* SREBP-dependent lipidomic reprogramming as a broad-spectrum antiviral target. *Nat Commun* **10**, 120, doi:10.1038/s41467-018-08015-x (2019).

50   Chan, J. F. *et al.* Simulation of the clinical and pathological manifestations of Coronavirus Disease 2019 (COVID-19) in golden Syrian hamster model: implications for disease pathogenesis and transmissibility. *Clin Infect Dis*, doi:10.1093/cid/ciaa325 (2020).

51   Chan, J. F. *et al.* Surgical mask partition reduces the risk of non-contact transmission in a golden Syrian hamster model for Coronavirus Disease 2019 (COVID-19). *Clin Infect Dis*, doi:10.1093/cid/ciaa644 (2020).

52   Chan, J. F. *et al.* Improved molecular diagnosis of COVID-19 by the novel, highly sensitive and specific COVID-19-RdRp/Hel real-time reverse transcription-polymerase chain reaction assay validated in vitro and with clinical specimens. *J Clin Microbiol*, doi:10.1128/JCM.00310-20 (2020).

53   Chu, H. *et al.* Middle East Respiratory Syndrome Coronavirus Efficiently Infects Human Primary T Lymphocytes and Activates the Extrinsic and Intrinsic Apoptosis Pathways. *J Infect Dis* **213**, 904-914, doi:10.1093/infdis/jiv380 (2016).
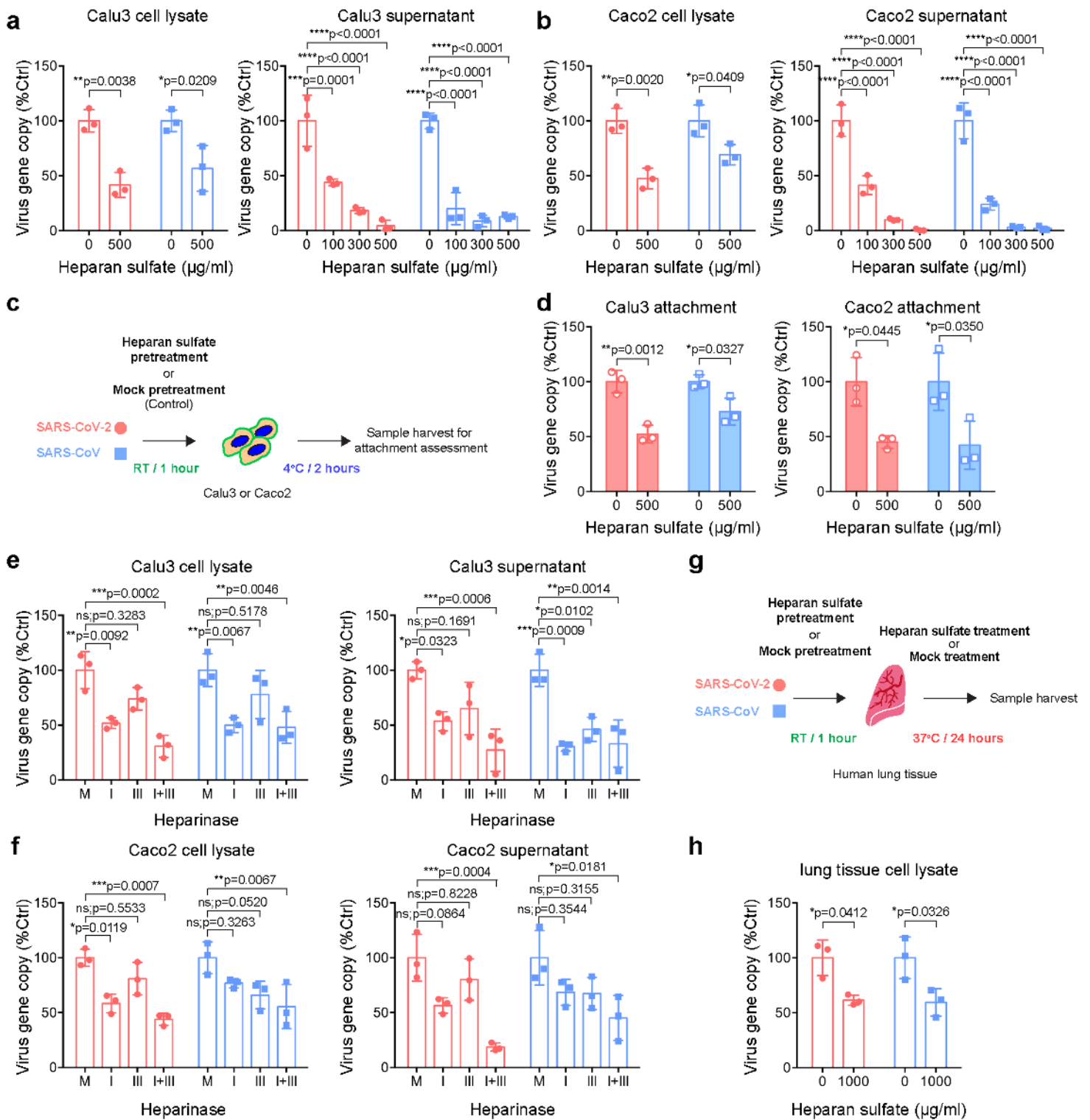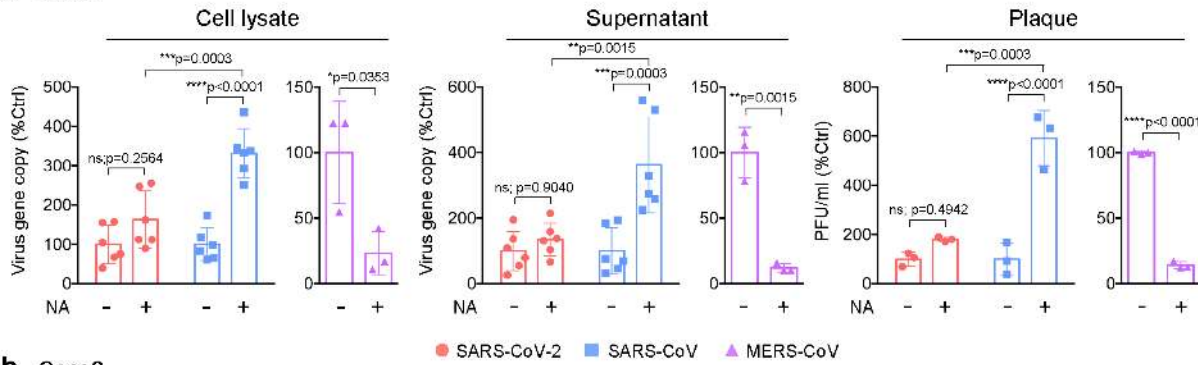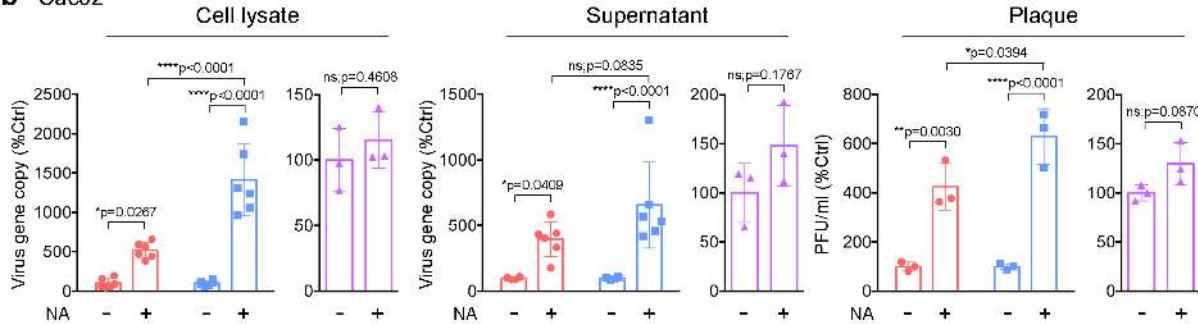
Figures

Figure 1

Heparan sulfate (HS) serves as an attachment factor for SARS-CoV-2 infection. a-b Calu3 and Caco2 cells were inoculated with HS-pretreated SARS-CoV-2 or SARS-CoV at 0.2MOI for 2h at 37°C. Cell lysates and supernatants were harvested at 24hpi and virus replication was determined with qRT-PCR. c Schematic of the attachment assay. d Calu3 and Caco2 cells were inoculated with HS-pretreated SARS-CoV-2 or SARS-CoV at 0.2MOI for 2h at 4°C. Cell lysates were harvested after the 2h incubation and virus attachment was determined with qRT-PCR. e-f Calu3 and Caco2 were pretreated with Heparinase I

(4U/ml), Heparinase III (0.5U/ml) or both for 1h at 37 °C, followed by virus infection at 0.2MOI. Cell lysates and supernatants were harvested at 24hpi for qRT-PCR analysis. g-h Human lung tissues were challenged with HS-pretreated SARS-CoV-2 or SARS-CoV at an inoculum of 1×107PFU/ml for 2h. Tissues were harvested and homogenized at 24hpi for viral gene copy detection. Data represented mean and standard deviations from three individual experiments. Statistical significance between groups was determined with two way-ANOVA. * indicated $p < 0.05$, ** represented $p < 0.01$, *** represented $p < 0.001$, **** represented $p < 0.0001$. ns = not significant.
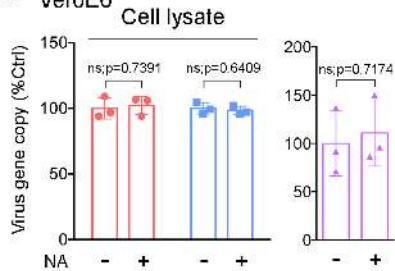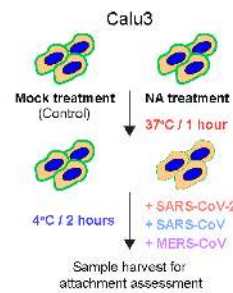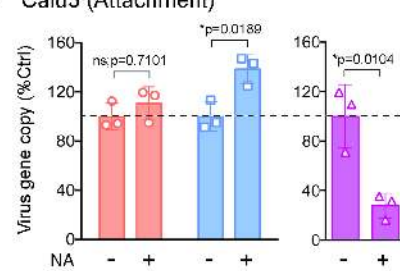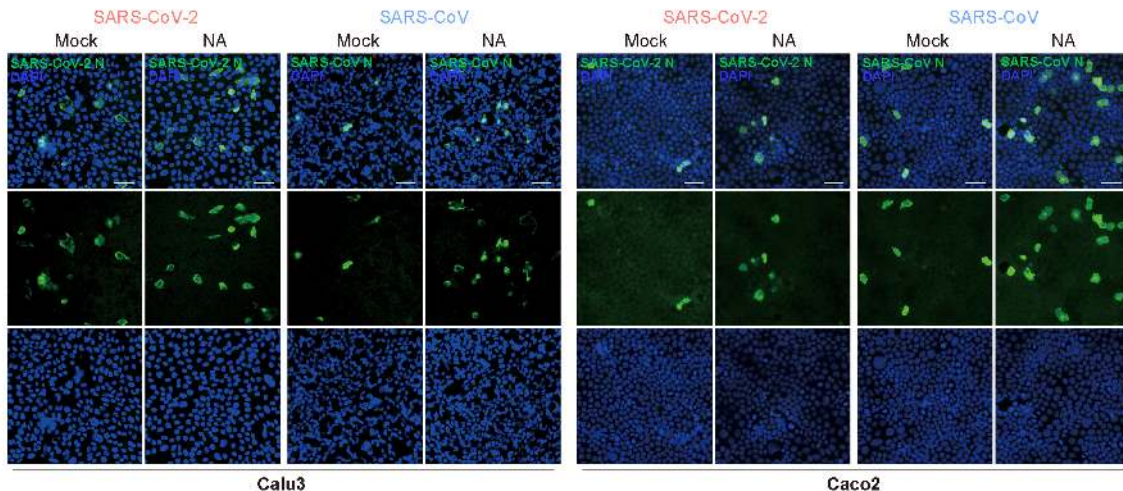
Figure 2

Sialic acids play differential roles on attachment and replication of SARS-CoV-2, SARS-CoV, and MERS-CoV. a-c Calu3, Caco2, and VeroE6 cells were treated with neuraminidase (NA) for 1h at 37°C, followed by SARS-CoV-2, SARS-CoV, or MERS-CoV inoculation at 0.2MOI for 2h. Cell lysates and supernatants were harvested at 24hpi for qRT-PCR analysis and plaque assay titration. d Schematic of attachment assay. e NA-pretreated Calu3 cells were incubated with the viruses at 4°C for 2h. Cell lysates were harvested at 2hpi for qRT-PCR analysis. f NA- or mock-treated Calu3 or Caco2 cells were challenged with SARS-CoV-2 or SARS-CoV at 0.2MOI. Infected cells were fixed at 16hpi and immunolabeled for virus nucleocapsid (N) protein (green) and DAPI (blue). Images were taken at 20× magnification. Bars represented 50μm. Data represented mean and standard deviations from three individual experiments. Statistical significance between groups was determined with two way-ANOVA or Student's t-test. * indicated $p < 0.05$, ** represented $p < 0.01$, *** represented $p < 0.001$, **** represented $p < 0.0001$. ns = not significant.
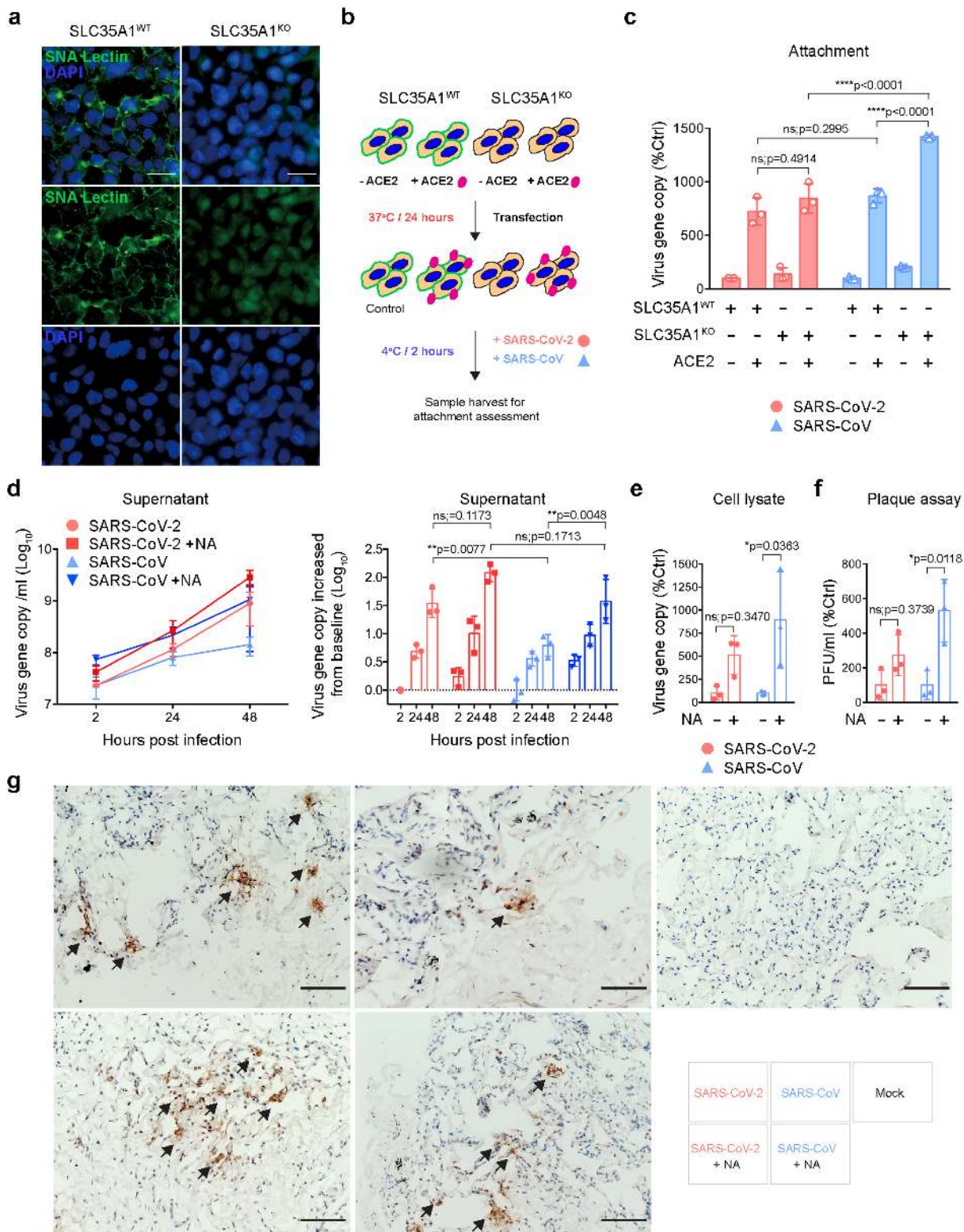
Figure 3

SARS-CoV-2 overcomes sialic acid-mediated restriction in ex vivo human lung tissues. a SLC35A1WT and SLC35A1KO 293 cells were fixed and stained with Sambucus Nigra Lectin (green) and DAPI (blue) for cell surface sialic acid detection. Bars represented 50μm. b Schematic of attachment assay. c SLC35A1WT and SLC35A1KO 293 cells with or without hACE2 overexpression were inoculated with SARS-CoV-2 or SARS-CoV at 0.2MOI for 2h at 4°C. Cell lysates were harvested at 2hpi for qRT-PCR analysis. d-e Mock- or

NA-treated ex vivo human lung tissues were infected with SARS-CoV-2 or SARS-CoV at an inoculum of 1×107PFU/ml. Supernatants were collected at 2, 24, and 48hpi and tissue samples were collected at 48hpi for qRT-PCR analysis. f Supernatants at 48hpi were titrated by plaque assays. g Representative images of human lung tissues challenged with SARS-CoV-2 or SARS-CoV with or without NA treatment. Viral N proteins were detected with anti-SARS-CoV-2-N or rabbit anti-SARS-CoV-N immune serum (arrows). Bars represented 100μm. Data represented mean and standard deviations from three individual experiments. Statistical significance between groups was determined with two way-ANOVA. * indicated p < 0.05, ** represented p < 0.01, *** represented p < 0.001, **** represented p < 0.0001. ns = not significant.
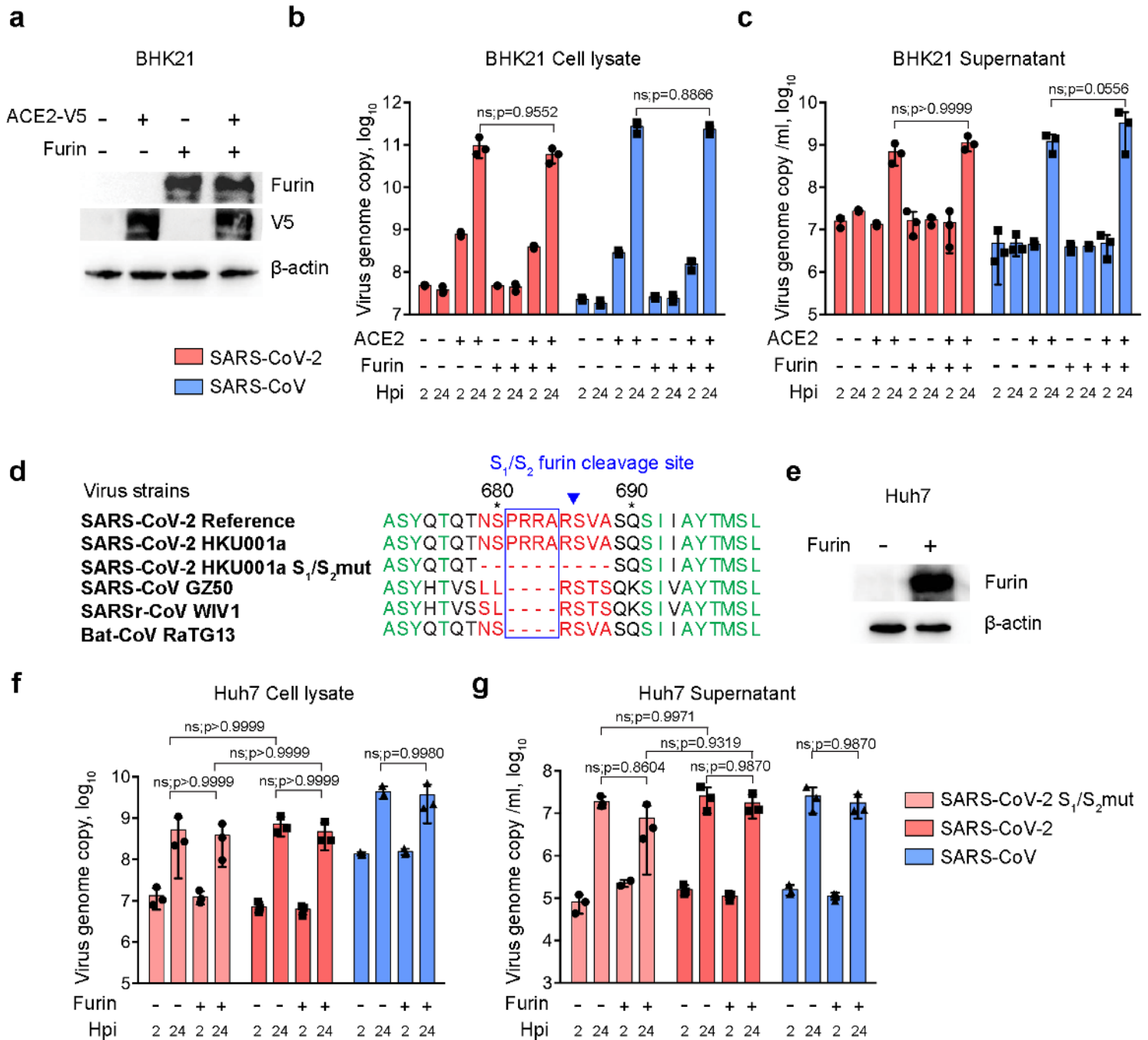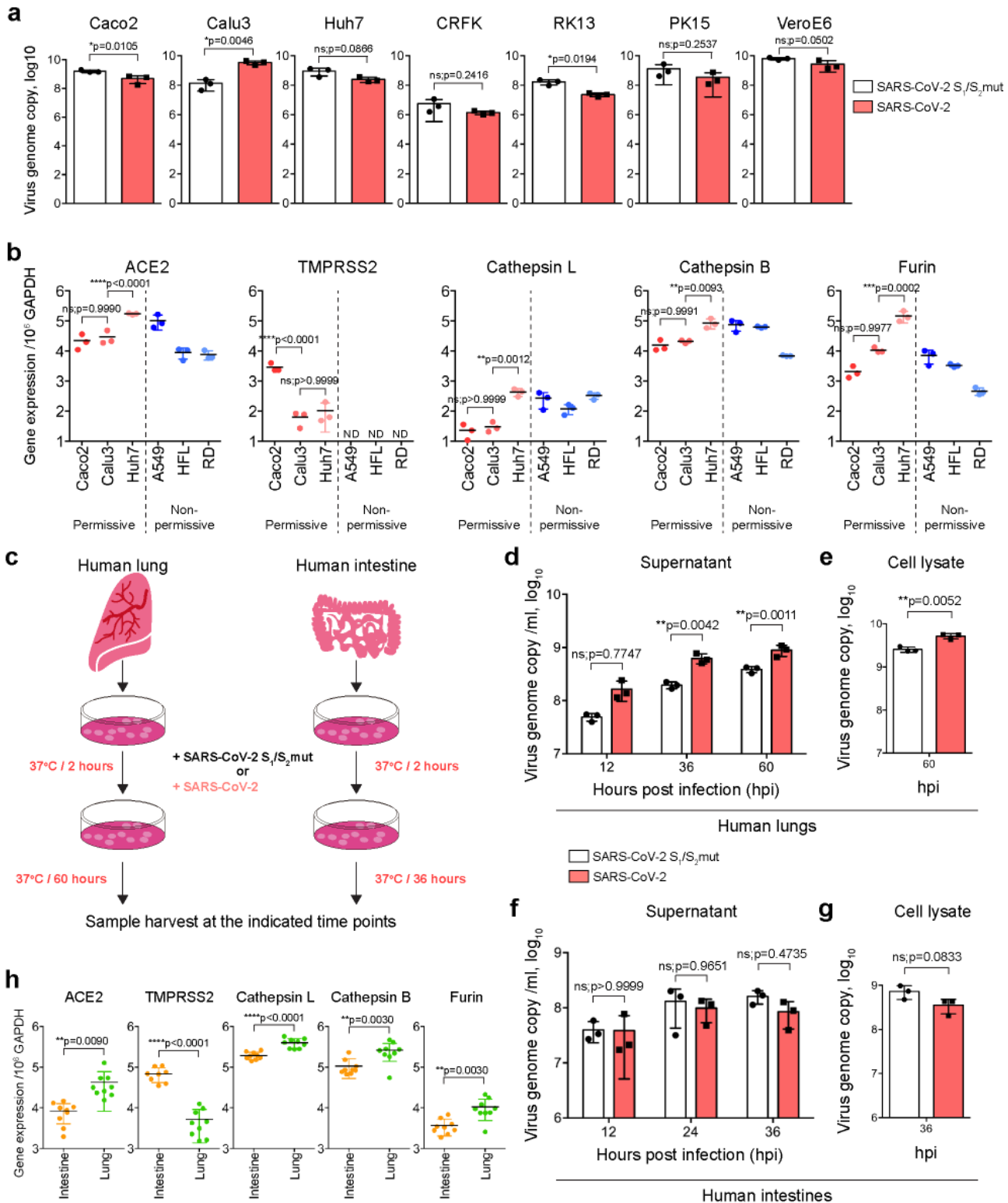

Figure 4

The inserted furin-like cleavage site or furin overexpression does not promote SARS-CoV-2 replication in BHK21 (non-permissive) and Huh7 (permissive) cells. a Human ACE2 and furin overexpression in BHK21 cells was confirmed with Western blot. b-c BHK21 cells with or without human ACE2 or furin overexpression were infected with SARS-CoV-2 or SARS-CoV. Cell lysates and supernatants were collected at 2 and 24hpi for qRT-PCR analysis. d Amino acid sequence alignment of residues around the S1/S2 cleavage site of SARS-CoV-2 reference strain (GenBank accession number: MN908947), SARS-CoV-2 HKU001a (MT230904), SARS-CoV-2 HKU001a S1/S2mut (MT621560), SARS-CoV GZ50 (AY304495), SARSr-CoV WIV1 (KF367457), and bat-CoV RaTG13 (MN996532). e Furin overexpression in Huh7 cells was confirmed with Western blot. f-g Huh7 cells with or without furin overexpression were infected with SARS-CoV-2, SARS-CoV-2 S1/S2mut, or SARS-CoV. Cell lysates and supernatants were collected at 2 and 24hpi for qRT-PCR analysis. Data represented mean and standard deviations from three individual experiments. Statistical significance between groups was determined with two way-ANOVA. ns = not significant.

Figure 5

The furin-like cleavage site in SARS-CoV-2 spike is required for efficient SARS-CoV-2 replication in ex vivo human lung. a Seven cell types of human and non-human origin, including Caco2 (human intestine), Calu3 (human lung), Huh7 (human liver), CRFK (cat), RK13 (rabbit), PK15 (pig), and VeroE6 (monkey) were infected with SARS-CoV-2 or SARS-CoV-2 S1/S2mut at 0.2MOI. Cell lysates were collected at 24hpi for viral genome copy analysis by qRT-PCR. b The expression of ACE2, TMPRSS2, cathepsin L, cathepsin

B, and furin from three representative permissive cell types (Caco2, Calu3, Huh7) and three non-permissive cell types (A549, HFL, RD) to SARS-CoV-2 replication was analyzed with qRT-PCR. c Schematic of ex vivo human lung and intestine tissue infection. d-g Human lung and intestine tissues were infected with SARS-CoV-2 or SARS-CoV-2 S1/S2mut. Cell lysate and supernatant samples were harvested at the indicated time points for qRT-PCR analysis. h The expression of ACE2, TMPRSS2, cathepsin L, cathepsin B, and furin from human lung and intestine tissues were determined with qRT-PCR. Data represented mean and standard deviations from three individual experiments. Statistical significance between groups was determined with two way-ANOVA or Student's t-test. * indicated $p < 0.05$, ** represented $p < 0.01$, *** represented $p < 0.001$, **** represented $p < 0.0001$. ns = not significant.
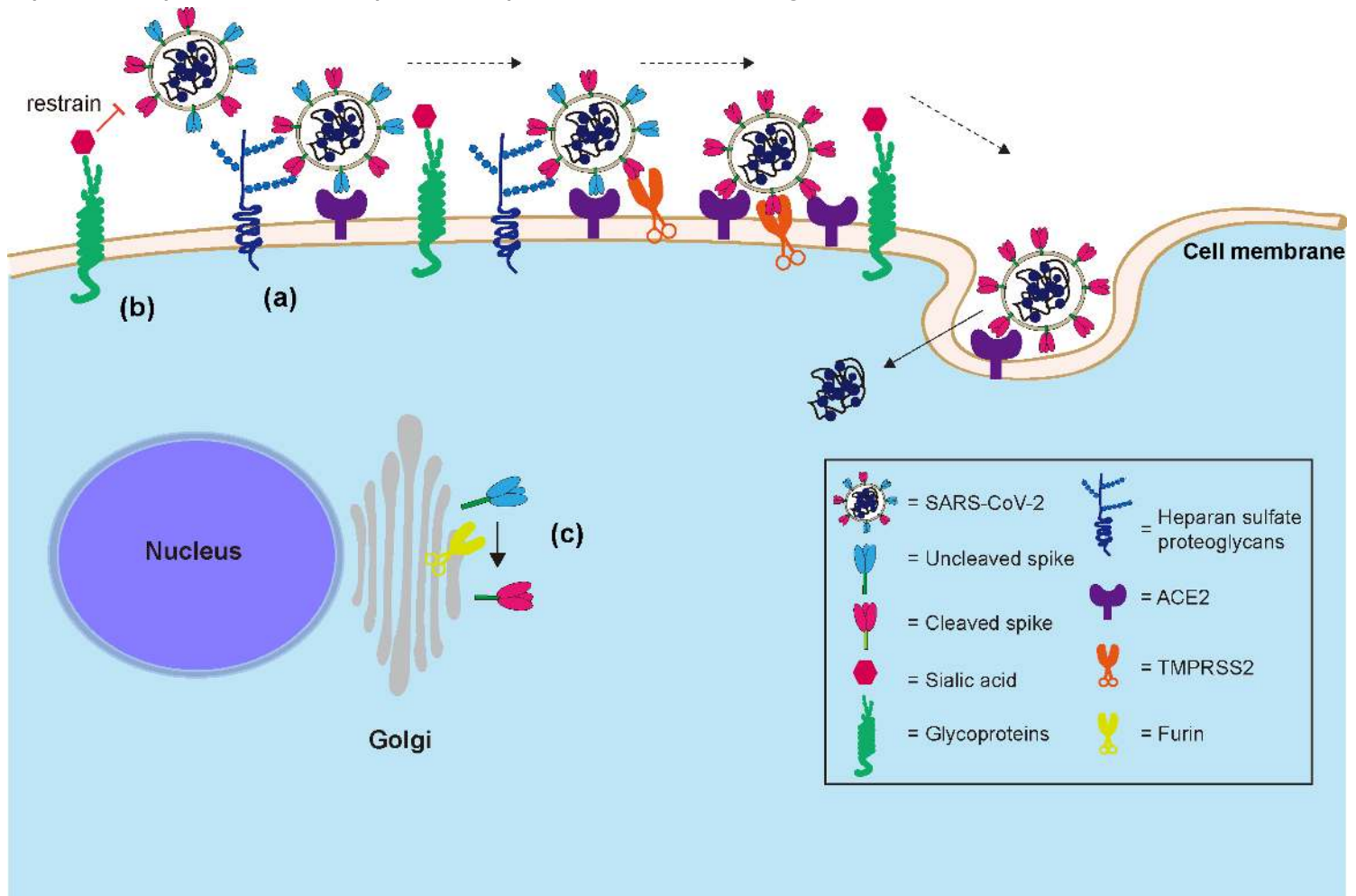

Figure 6

Schematic of the host and viral determinants for SARS-CoV-2 infection of the human lung as revealed in this study. a SARS-CoV-2 can utilize cell surface heparan sulfate proteoglycan as an attachment receptor. b SARS-CoV-2 can largely overcome sialic acid-mediated restriction in lung cells. c Furin cleavage of SARS-CoV-2 spike is essential for efficient SARS-CoV-2 replication in the human lung, which is potential due to the relatively low level of ACE2 expression in the lung comparing to many other human tissues.

Supplementary Files

This is a list of supplementary files associated with this preprint. Click to download.

- ChuetalSARSCoV2EntrydeterminantsFigureS1.tif
- ChuetalSARSCoV2EntrydeterminantsFigureS2.tif